Petrological and geochemical characteristics of metamorphic and igneous units from the allochthonous Madre de Dios Terrane, Southern Chile

F.A. Sepúlveda [a,*], F. Hervé [a], M. Calderón [a], J.P. Lacassie [b,c]

[a] *Departamento de Geología, Facultad de Ciencias Físicas y Matemáticas, Universidad de Chile, Casilla 13518, Correo 21, Santiago, Chile*
[b] *Paleoproterozoic Mineralization Research Group, Department of Geology, University of Johannesburg, Auckland Park, Johannesburg, 2006, South Africa*
[c] *SERNAGEOMIN, Av. Santa María 0104, Providencia, Santiago, Chile*

Abstract

The Denaro Complex, part of the Madre de Dios Terrane is composed of metamorphosed pillow basalts, metahyaloclastites, banded metalliferous and radiolarian metacherts, metapelites and redeposited calcareous metasandstones. The basaltic rocks show primary textures, minerals and structures. They are foliated especially in the vicinities of thrust faults, interpreted to have developed during the accretion of the terrane to the Gondwana margin. Composition of relic primary augite and chromite crystals plots into the MORB field of tectonic discriminant diagrams, as do the analyses of whole rock geochemistry, which indicates that these rocks are akin to volcanic rocks erupted along a constructive plate margin (N- and E-type MORBs), probably in a spreading axis-centered oceanic plateau or ridge. The metamorphic assemblages of pumpellyite–actinolite facies bear witness of metamorphism in a frontal accretionary wedge at elevated *P* and low *T* conditions, probably related to the Late Triassic–Early Jurassic Chonide event, which has been recognized elsewhere in the Patagonian Andes.

Keywords: Metamorphism; Terrane accretion; Pumpellyite–actinolite facies; Seamount subduction; Frontal accretion

1. Introduction

1.1. Geological background

The basement of the Patagonian Andes is composed of an assemblage of accretionary complexes forming the palaeo-Pacific margin of Gondwana, mainly of pre-Early Jurassic age, but with different structural and metamorphic histories (Forsythe, 1982; Thomson and Hervé, 2002). However, this hypothesis has been difficult to demonstrate because the complexes were disrupted and separated by the intrusion of the Late Jurassic to Cenozoic Patagonian Batholith (Bruce et al., 1991; Pankhurst et al., 1999).

* Corresponding author.
E-mail address: fersepul@ing.uchile.cl (F.A. Sepúlveda).

The rocks which crop out at the Madre de Dios archipelago (50°–50°50'S), referred to by Hervé and Mpodozis (2005) as Madre de Dios Terrane (MDT), are an important portion of the western belt of outcrops of the Patagonian basement and consist of fragments of the accretionary complex built on the western margin of Gondwana during the Late Palaeozoic–Early Mesozoic (Fig. 1). The stratigraphical, geochemical and structural features of the units which comprise this macro-melange were studied in detail by Forsythe and Mpodozis (1979, 1983) who distinguished: the Denaro Complex (DC) formed by fragments of ocean floor and its sedimentary cover (Late Carboniferous–Early Permian, see Ling et al., 1985), the Tarlton Limestone (TL) formed by massive marine limestone with an age between Middle Pennsylvanian and Early Permian (Ceccioni, 1956; Douglass and Nestell, 1976), and the Duque de York Complex (DYC), formed by a succession of pelite, greywacke and conglomerate of continental provenance, and deposited uncomformably on top of DC and TL when these units approached the Gondwana continental margin. U–Pb

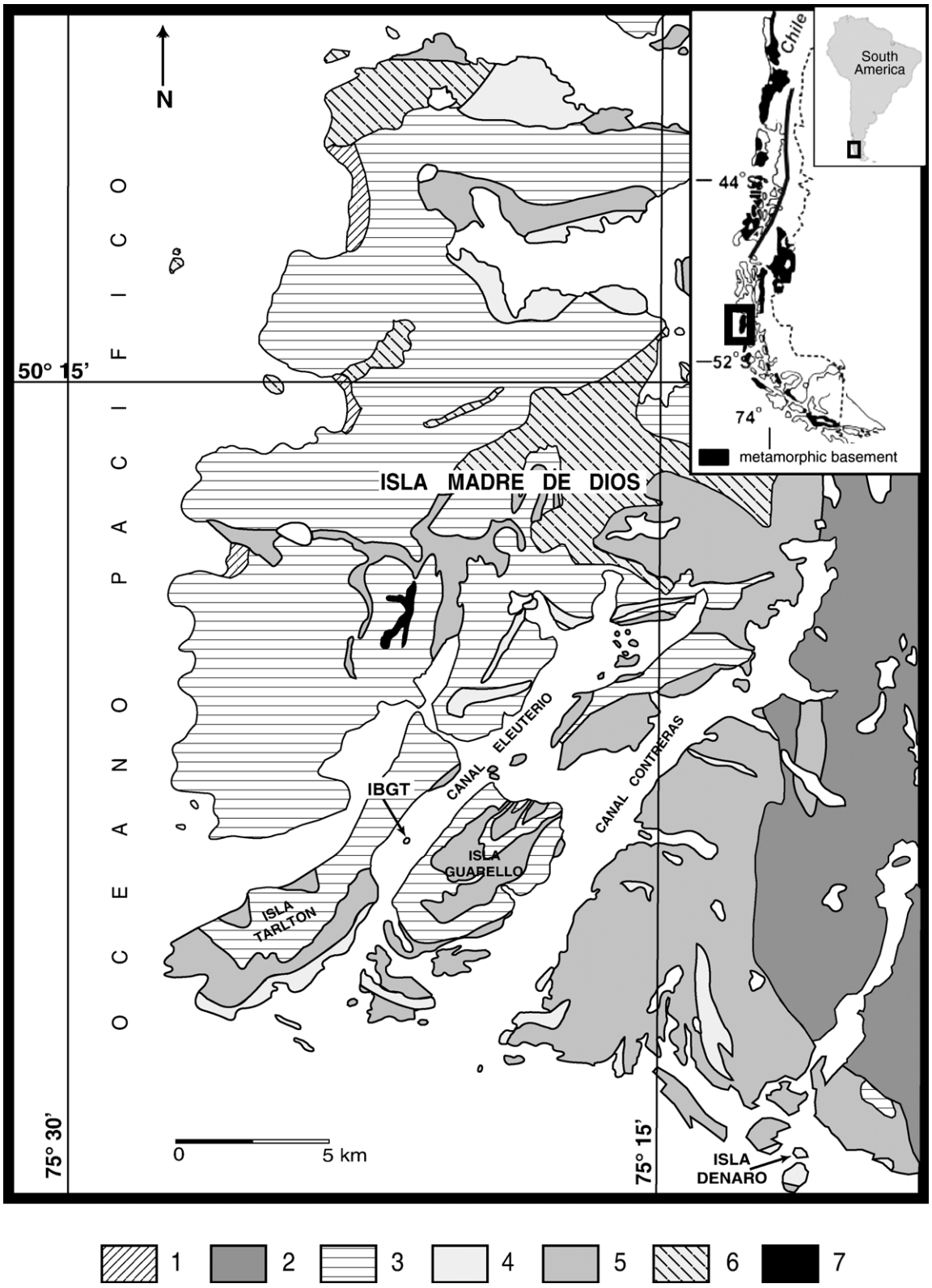

Fig. 1. Geological map of the studied area [modified from Forsythe and Mpodozis (1983) and Lacassie (2003)]. 1: Quaternary deposits. 2: South Patagonian Batholith (SPB). 3: Tarlton Limestone (TL). 4: Denaro Complex (DC). 5: Duque de York Complex (DYC). 6: Unmapped basement. 7: Sill.

SHRIMP detrital zircon ages from sandstones of the DYC reveal that the most abundant youngest population is late Early Permian (ca. 270 Ma) (Hervé et al., 2003). Zircon fission track data have allowed Thomson and Hervé (2002) to infer that metamorphism that affects the DYC, and probably also the underlying TL and DC, took place during or before the

Table 1
Geochemical whole rock data for samples of the Denaro Complex and cross-cutting dykes

	1	4	5	7	9	14	18	19	26	35	36	04_3	04_4	04_5	05_13	05_18	05_21	05_9	98_03J
	ICP-AES	ICP-AES	ICP-AES	ICP-AES	ICP-AES	ICP-AES	ICP-AES	ICP-AES	ICP-AES	ICP-AES	ICP-AES	XRF	XRF	XRF	XRF	XRF	XRF	XRF	XRF
	Pillow basalt	Pillow basalt	Pillow basalt	Pillow basalt	Pillow basalt	Pillow basalt	Basalt	Dyke	Hyaloclastite	Foliated pillow basalt	Pillow basalt	Pillow basalt	Pillow basalt	Pillow breccia	Dyke	Amigdaloidal basalt	Dyke	Dyke	Foliated hyaloclastite
SiO_2	44.50	50.35	47.24	47.25	50.67	50.50	45.06	50.64	46.20	49.10	50.50	43.00	49.87	49.90	51.79	41.09	50.37	48.03	46.60
TiO_2	1.67	1.85	0.96	1.14	2.19	1.08	1.28	1.86	0.41	1.15	1.10	0.75	1.08	1.01	1.72	1.25	1.98	2.29	0.62
Al_2O_3	16.24	13.72	14.40	14.68	13.41	12.82	15.31	14.69	22.44	14.44	13.35	13.16	11.16	9.85	12.45	15.33	13.72	10.16	13.87
Fe_2O_3	3.86	1.68	3.30	2.03	2.55	2.89	6.13	3.90	2.87	1.56	3.34								
FeO	11.40	10.12	6.80	8.72	9.64	8.00	4.00	8.80	2.84	9.64	6.48	12.25	13.27	13.94	14.33	9.74	12.65	14.18	9.78
MnO	0.20	0.14	0.16	0.16	0.14	0.16	0.11	0.26	0.08	0.13	0.19	0.15	0.18	0.20	0.22	0.13	0.21	0.11	0.15
MgO	7.52	6.79	8.13	10.22	7.32	8.12	8.01	4.07	5.64	8.70	9.78	14.85	11.74	11.17	5.51	24.15	3.71	9.16	16.99
CaO	5.38	4.52	12.32	6.45	6.33	10.50	7.38	3.09	8.37	8.19	8.11	8.73	6.77	8.82	6.85	6.98	7.28	6.32	6.12
Na_2O	2.70	3.25	2.75	3.40	2.95	2.38	2.66	4.52	2.35	2.98	1.82	1.68	2.38	2.40	3.55	0.76	3.29	2.18	3.22
K_2O	0.35	0.35	0.09	0.37	0.32	0.60	1.54	2.09	3.48	0.25	0.17	1.18	0.87	0.19	0.86	0.29	1.12	0.46	0.86
P_2O_5	0.14	0.23	0.10	0.10	0.23	0.10	0.18	0.35	0.05	0.11	0.10	0.09	0.09	0.08	0.36	0.15	0.42	0.27	0.09
LOI	5.94	6.78	3.84	5.31	4.43	3.38	8.77	4.77	5.21	4.33	5.30								
Total	99.90	99.78	100.09	99.83	100.18	100.53	100.43	99.04	99.94	100.58	100.24	96.09	97.56	97.68	97.79	99.87	94.75	93.31	98.28
La	3.50	3.50	2.00	1.00	14.00	1.00	8.00	14.00	1.00	1.00	1.00								
Ce	14.00	15.00	7.00	6.00	18.00	6.00	21.00	36.00	4.00	5.00	6.00								
Nd	12.00	12.00	7.00	7.00	14.00	7.00	15.00	24.00	4.00	7.00	6.00								
Sm	3.47	3.25	1.89	2.02	4.59	2.00	3.74	5.97	0.88	2.20	1.98								
Eu	1.29	1.24	0.78	0.79	1.37	0.73	1.21	1.83	0.15	0.74	0.76								
Gd	4.54	4.62	2.79	3.35	6.51	3.05	4.60	6.61	1.16	3.27	2.79								
Dy	5.70	5.65	3.51	3.97	7.27	3.70	5.31	5.94	1.20	3.63	3.36								
Ho	1.25	1.20	0.79	0.80	1.44	0.80	1.06	1.18	0.26	0.78	0.68								
Er	3.50	3.00	2.10	2.33	4.90	2.33	3.17	3.31	0.79	2.20	1.97								
Yb	3.66	2.90	2.11	2.45	4.27	2.33	312.00	3.26	0.90	2.25	1.92								
Lu	0.56	0.44	0.33	0.35	0.71	0.35	0.50	0.54	0.14	0.35	0.32								
Y	31	30	21	22	38	22	27	32	8	23	18	18.2	23	18.1	24.3	20.4	29.3	25.2	15.3
Sc	52	48	45	52	48	51	41	36	31	49	46								
Hf	2.51	3.4	1.5	2.4	3.9	1.8	1.7	3.6	1	1.7	1.7								
Th	1	1	1	1	2	1	1	2	1	1	1								
Nb	11	12	6	7	12	7	20	12	5	12	6	3.2	4.9	2.4	7.6	16.9	8.6	9.5	8.5
Zn	108	124	90	76	106	92	74	110	45	87	71	94.4	106.5	106.3	99.9	125.1	116.9	151	100.3
Co	50	50	38	40	48	38	31	33	18	34	26	51.1	57.4	56.2	50.3	55	48.2	46	54.2
Ni	54	48	95	70	43	63	79	16	53	52	70	149.2	95.1	82.7	14	226.8	16.9	10.9	281.3
Ba	400	1970	103	210	185	312	100	10700	162	159	137	845.5	574.8	107.2	246.7	77.6	340.2	245.9	41.6
Cr	19	112	293	258	58	126	249	20	226	77	215	554.2	225.5	210	101.4	618.5	99.3	74.1	1103.3
V	440	400	274	290	400	315	227	351	141	290	271	220.1	321.9	295	414.4	281.3	351.8	482.3	202.5
Cu	248	159	167	141	150	137	35	182	22	138	128	89.8	153.6	198.4	175.8	102.3	187	233.4	223.6
Rb												29	33.5	5.5	17.6	4.6	33	12.7	12.1
Sr	340	160	320	115	320	235	74	337	400	217	108	446.5	81.2	232.9	322.7	487	339.5	300.5	198.8
Zr	71	95	45	54	120	50	76	133	26	55	49	70.1	45.8	48.8	110.3	99.4	128.9	124	39.4

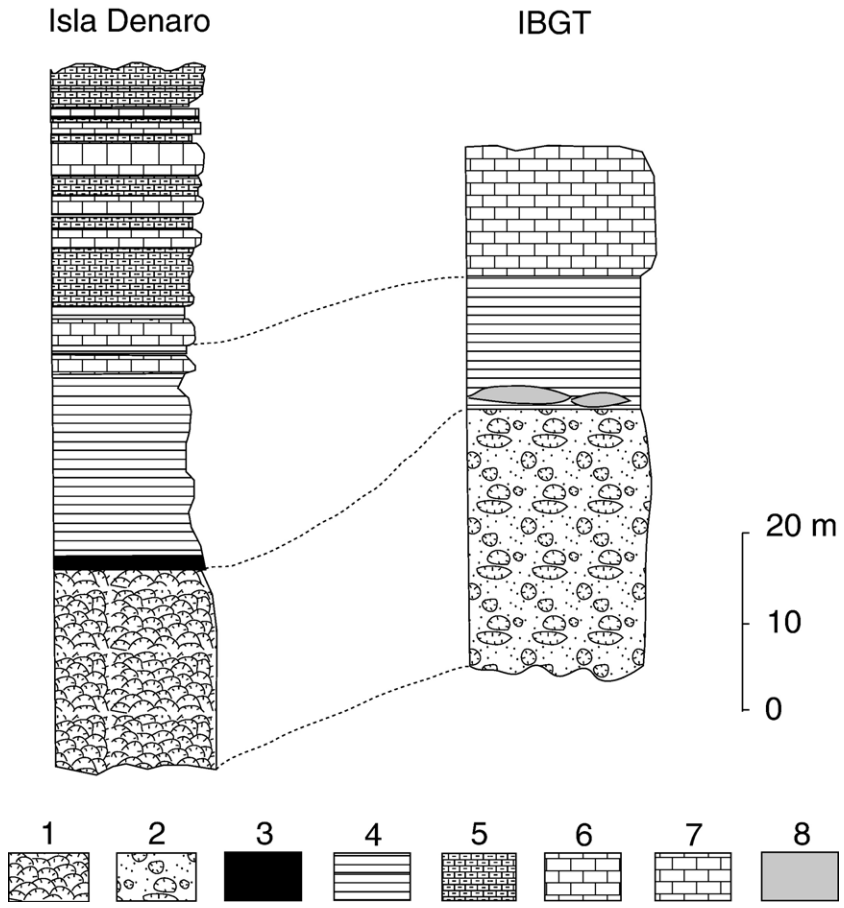

Fig. 2. Stratigraphic columns of the Denaro Complex from Isla Denaro and site IBGT (island between Guarello and Tarlton) (after Forsythe and Mpodozis, 1983). 1) pillow basalts; 2) hyaloclastites; 3) metalliferous cherts; 4) banded cherts; 5) siliceous shales and calcarenites; 6) reworked limestones; 7) limestones (TL); 8) metalliferous sediments.

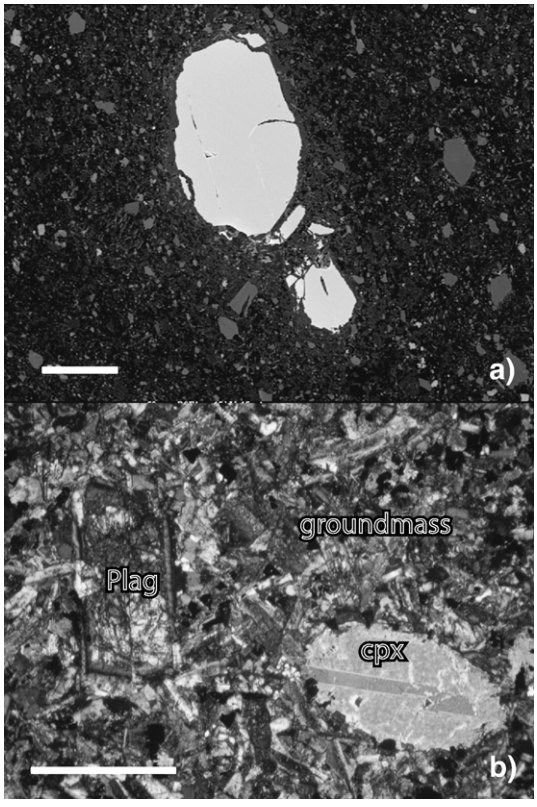

earliest Jurassic, prior to the emplacement of the South Patagonian Batholith (SPB) in the Early Cretaceous in this area, which has isotopic ages closest to the contact with the MDT of 133–112 Ma (Rb–Sr whole rock and biotite isochron, Halpern, 1973), 130–143 Ma (K–Ar biotite, Duhart et al., 2003) and ca. 133 Ma (U–Pb SHRIMP zircon, Hervé et al., 2007a).

On the other hand, Forsythe and Mpodozis (1983) concluded that the DC is composed of fragments of oceanic floor that migrated from an active ridge and was progressively covered by silicic planktonic detritus (banded cherts). Hervé et al. (1999a) considered that the metabasalts of this complex correspond to E-MORB basalts coming from a mid-ocean ridge or an oceanic plateau. These interpretations point towards the idea that the DC basalts would have been affected by ocean floor metamorphism prior to their accretion. Sepúlveda (2004), however, concluded that the metamorphic mineral paragenesis was formed under a *P–T* regime typical of a subduction zone environment (accretionary prism), which implies that

Fig. 3. Microphotographs of selected samples. a) Back scattered electrons image of relic chromite crystals in metahyaloclastite sample. White horizontal line represents 50 μm. b) Plane polarized view of the characteristic textures of dykes. White horizontal line represents 1 mm.

this process probably erased any early evidence of a sea-floor metamorphism. The conditions of the metamorphism developed in the accretionary wedge may have been further modified by contact metamorphism produced by the intrusion of the SPB.

1.2. Palaeogeographic setting

Current palaeogeographic reconstructions for the Late Carboniferous–Early Permian place the portion of the Gondwana margin where the Madre de Dios archipelago is presently

Table 2
Representative relic mineral analyses (chromite stoichiometry calculated using the procedure of Barnes and Roeder (2001), using the correction of C–J De Hoog)

	Chromite[1]										
	Rim	Rim	Core	Rim	Core	Rim	Rim	Core	Rim	Rim	Rim
	983_1	983_58	983_59	983_69	983_70	983_71	984_57	984_58	984_59	984_116	984_117
SiO_2	0.04	0.10	0.12	0.10	0.05	0.11	0.12	0.10	0.09	0.13	0.11
TiO_2	0.22	0.22	0.21	0.26	0.22	0.43	0.18	0.15	0.19	0.11	0.17
Al_2O_3	20.99	20.87	21.23	22.51	22.84	22.57	20.44	20.19	20.56	20.72	21.13
Cr_2O_3	46.54	46.70	46.66	42.38	43.58	41.36	47.42	47.91	47.63	48.24	47.52
Fe_2O_3	4.12	4.40	3.97	5.67	4.44	6.08	4.17	4.21	3.93	2.98	3.15
FeO	14.26	14.36	13.91	16.54	17.08	16.72	13.67	13.56	13.79	13.15	13.75
MnO	0.27	0.29	0.30	0.27	0.23	0.24	0.18	0.31	0.25	0.31	0.25
MgO	13.74	13.71	13.98	12.35	12.17	12.31	14.07	14.09	14.01	14.22	14.00
CaO	0.01	0.03	0.00	0.10	0.04	0.13	0.03	0.02	0.00	0.01	0.02
Na_2O	0.01	0.01	0.00	0.01	0.03	0.02	0.00	0.00	0.02	0.00	0.01
K_2O	0.00	0.03	0.00	0.03	0.02	0.01	0.00	0.01	0.00	0.01	0.01
Total	99.79	100.27	99.98	100.22	100.27	99.97	100.27	100.54	100.48	99.87	100.12
Si	0.001	0.003	0.004	0.003	0.002	0.003	0.004	0.003	0.003	0.004	0.003
Ti	0.005	0.005	0.005	0.006	0.005	0.010	0.004	0.004	0.004	0.003	0.004
Al	0.762	0.755	0.768	0.820	0.828	0.825	0.741	0.732	0.744	0.752	0.765
Cr	1.133	1.133	1.131	1.036	1.059	1.013	1.154	1.164	1.156	1.174	1.154
Fe^{3+}	0.095	0.102	0.092	0.132	0.103	0.142	0.097	0.097	0.091	0.069	0.073
Fe^{2+}	0.367	0.369	0.357	0.428	0.439	0.434	0.352	0.349	0.354	0.338	0.353
Mn	0.007	0.007	0.008	0.007	0.006	0.006	0.005	0.008	0.006	0.008	0.006
Mg	0.630	0.627	0.639	0.569	0.558	0.569	0.645	0.645	0.641	0.652	0.641
Total	3.000	3.001	3.002	3.001	2.999	3.002	3.001	3.001	3.000	3.000	3.000
$\#Fe^{3+}$	0.048	0.051	0.046	0.066	0.052	0.072	0.048	0.049	0.046	0.035	0.037

	Clinopyroxene											
	983_12	983_14	983_15	983_21	983_23	983_44	983_47	983_51	983_56	983_62	983_67	983_96
SiO_2	49.96	51.76	50.70	51.01	50.55	51.56	51.33	52.41	50.98	51.71	51.31	51.28
TiO_2	0.59	0.46	0.55	0.52	0.53	0.59	0.24	0.19	0.31	0.26	0.22	0.37
$Al2O_3$	2.60	2.29	3.04	3.20	3.53	2.37	3.12	1.84	3.24	2.73	2.52	3.24
Cr_2O_3	0.09	0.16	0.38	0.28	0.63	0.05	1.23	0.80	1.52	1.31	1.10	0.45
FeO	12.48	8.55	7.82	7.35	6.29	11.69	5.60	5.54	5.69	6.42	5.28	7.40
MnO	0.37	0.24	0.15	0.18	0.17	0.30	0.16	0.15	0.18	0.21	0.17	0.18
MgO	15.74	17.43	16.89	17.31	16.37	15.37	17.28	18.72	16.92	17.33	17.74	18.52
CaO	16.24	18.06	19.16	18.89	20.38	18.17	19.88	19.55	20.14	19.23	19.77	17.57
Na_2O	0.16	0.14	0.21	0.28	0.20	0.19	0.35	0.21	0.40	0.40	0.20	0.17
K_2O	0.01	0.02	0.01	0.04	0.04	0.02	0.00	0.00	0.01	0.02	0.00	0.02
Total	98.24	99.08	98.90	99.06	98.70	100.30	99.17	99.40	99.38	99.61	98.31	99.20
Si	1.895	1.919	1.882	1.884	1.878	1.916	1.889	1.917	1.876	1.899	1.902	1.884
Ti	0.017	0.013	0.015	0.014	0.015	0.016	0.007	0.005	0.008	0.007	0.006	0.010
Al	0.116	0.100	0.133	0.139	0.155	0.104	0.135	0.079	0.141	0.118	0.110	0.140
Cr	0.003	0.005	0.011	0.008	0.018	0.001	0.036	0.023	0.044	0.038	0.032	0.013
Fe^{3+}	0.070	0.042	0.078	0.077	0.059	0.044	0.063	0.068	0.075	0.061	0.055	0.070
Fe^{2+}	0.328	0.224	0.166	0.151	0.138	0.321	0.111	0.102	0.101	0.137	0.109	0.158
Mn	0.012	0.007	0.005	0.006	0.005	0.010	0.005	0.005	0.006	0.007	0.005	0.006
Mg	0.890	0.963	0.934	0.953	0.906	0.851	0.947	1.021	0.928	0.948	0.980	1.014
Ca	0.660	0.717	0.762	0.747	0.811	0.724	0.784	0.766	0.794	0.757	0.786	0.692
Na	0.011	0.010	0.015	0.020	0.014	0.014	0.025	0.015	0.028	0.028	0.015	0.012
K	0.001	0.001	0.001	0.002	0.002	0.001	0.000	0.000	0.000	0.001	0.000	0.001
Total	4.002	4.001	4.002	4.001	4.001	4.001	4.001	4.001	4.001	4.001	4.001	4.001

For details see http://www.em.csiro.au/terrain_studies/aboutus/people/stephen_barnes/roeder_spinels.htm.
[1] Fe^{3+} content in chromites was determined by using stoichiometry and an ideal XY_2O_4 formula, where X=(Fe^{2+}, Ni, Mn, Co, Zn) and Y=(Cr^{3+}, Fe^{3+}, Al); Fe is subdivided into Fe^{2+} and Fe^{3+} to satisfy the condition $n_Y=2n_X$ where n_Y is total atoms of trivalent cations, and n_X is total divalent cations per unit cell.

located at a high southern latitude, well outside the tropical zone where the TL is likely to have been deposited (Lacassie, 2003). This fact, together with the contemporaneity of the TL with the ocean floor deposit of the DC (Ling et al., 1985) lead to the conclusion that the MDT represents an allochthonous terrane originated at lower latitudes (around 20°S) and accreted via subduction processes to Gondwana after the Permian (Hervé et al., 2000). Lacassie (2003), following the interpretations of Hada et al. (2001) and Cawood et al. (2002), pointed out that the accretion of the TL and the DC would have occurred against a different sector of the Gondwana margin than the one occupied today, from where it would have been displaced by dextral translation, as a coherent block. The timing of the accretion of these units is bracketed between the age of deposition of the DYC, ca. 270 Ma (the youngest detrital zircon U–Pb SHRIMP age component) and the minimum age of metamorphism, 195 Ma (fission track detrital zircon age).

Palaeomagnetic data on the TL and the DC (Rapalini et al., 2001) indicate that, after Early Cretaceous remagnetization produced by the thermal influence of the SPB, both units underwent a counter-clockwise rotation of ca. 117° with an inappreciable latitudinal change. This evidence allowed Rapalini et al. (2001) to conclude (taking into account the structural studies of Forsythe and Mpodozis, 1979, 1983) that these rock units had been accreted to the Gondwana margin from the NW rather than from the SW as had been previously suggested (Forsythe and Mpodozis, 1983). This interpretation is consistent with the sinistral sense of shear of main structures parallel to the margin of South America, and is also coherent with the migration of the Antarctic Peninsula toward the South. It is, however, contrary to the hypothesis of Lacassie (2003). In addition, it is suggested that the end Triassic deformation in the northern Antarctic Peninsula, which affects the Trinity Peninsula Group accretionary complex, is associated with sinistral shearing, while dextral shearing is mainly a Cretaceous phenomenon in the Antarctic Peninsula (A. Vaughan, October 2006, written communication).

1.3. Aims of this study

The purpose of this paper is to present information bearing on the tectonic setting of formation and metamorphism of the basalts of the DC, based on relic and metamorphic mineral chemistry, respectively. In addition, data on the geochemistry and petrography of dykes which crosscut the MDT constrain its evolution and possible connection with the SPB.

2. Analytical methods

Eleven ICP-AES and eight wavelength-dispersive XRF analyses of metamorphosed pillow basalts and metahyaloclastites from the DC and cross-cutting dykes (Table 1) were performed at the Department of Geology, University of Chile and at the SPECTRAU Laboratory, Department of Geology, University of Johannesburg, South Africa, respectively.

The XRF analyses were carried out on Philips Magix Pro Spectrometer equipment. The major and the trace elements were analysed on lithium borate ($Li_2B_4O_7$– $LiBO_2$) fused glass beads and pressed powder pellets, respectively. The accuracy and precision of the data were estimated from repeated analyses of certified reference materials (basaltic rocks BE-N and JB-3). The accuracy was found to be better than ±5% for SiO_2, TiO_2, $A1_2O_3$, CaO, MgO, MnO, K_2O, Na_2O, P_2O_5 and for total Fe_2O_3; ±4% for Nb, Zn, Co, Ni, Ba, Cu, Rb, Sr and Zr; and ±10% for Cr, V and Y. Precision for all major oxides was always better than 0.5%; for trace elements it was better than 3%.

EPMA analyses of two samples of metabasalts of the DC were obtained using a CAMECA SX 100 at Stuttgart Universität, Germany. Operation conditions were an acceleration voltage of 15 kV, a beam current of 15 nA, 20 s counting time per element and a defocused beam of 8 μm in order to avoid loss of alkalies in mica and amphibole.

3. Petrography and mineral chemistry

The Denaro Complex is constituted by a succession of unknown thickness of metamorphosed pillow basalts, metahyaloclastites, banded metalliferous and radiolarian metacherts, metapelites and redeposited calcarenites (Fig. 2). The metabasalts and metahyaloclastites have primary pillow structures with porphyritic to subophitic hypidiomorphic textures, frequently with amygdales. They are partly transformed to foliated greenschists in some localities. The samples analysed by EPMA are metabasaltic and hyaloclastitic semi-schists from an outcrop where DC and TL are in contact by a thrust fault. The rocks contain relic igneous clinopyroxene and chromite crystals preserved within a metamorphic mineralogy (Fig. 3a).

The cross-cutting dykes have an unaltered aspect in comparison with the metabasalts that belong to the DC, and display holocristaline, panidiomorphic, intergranular and porphyric textures. The phenocrystals present are pyroxenes and plagioclases in a groundmass composed of plagioclase, pyroxene, chloritised biotite and ilmenite crystals (Fig. 3b).

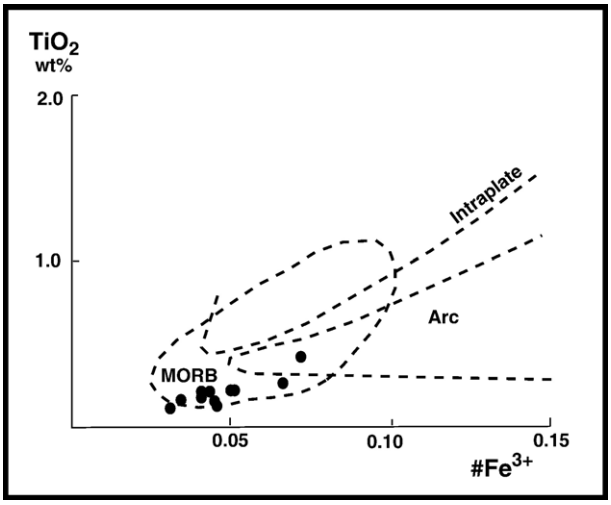

Fig. 4. Chromite plots. $\#Fe^{3+}$ vs. TiO_2 (Arai, 1992). $\#Fe^{3+}$ calculated as $Fe^{3+}/(Al+Cr+Fe^{3+})$.

3.1. Tectonic discriminant diagrams

The relic igneous crystals in the analysed metabasalts are clinopyroxenes (augites) and chromites. Representative analyses of relic igneous clinopyroxenes and chromites in metabasalts are shown in Table 2. The chromites plot in the MORB field of the discriminant diagram of Arai (1992) (Fig. 4), and in the ocean floor basalts field in the diagrams of Barnes and

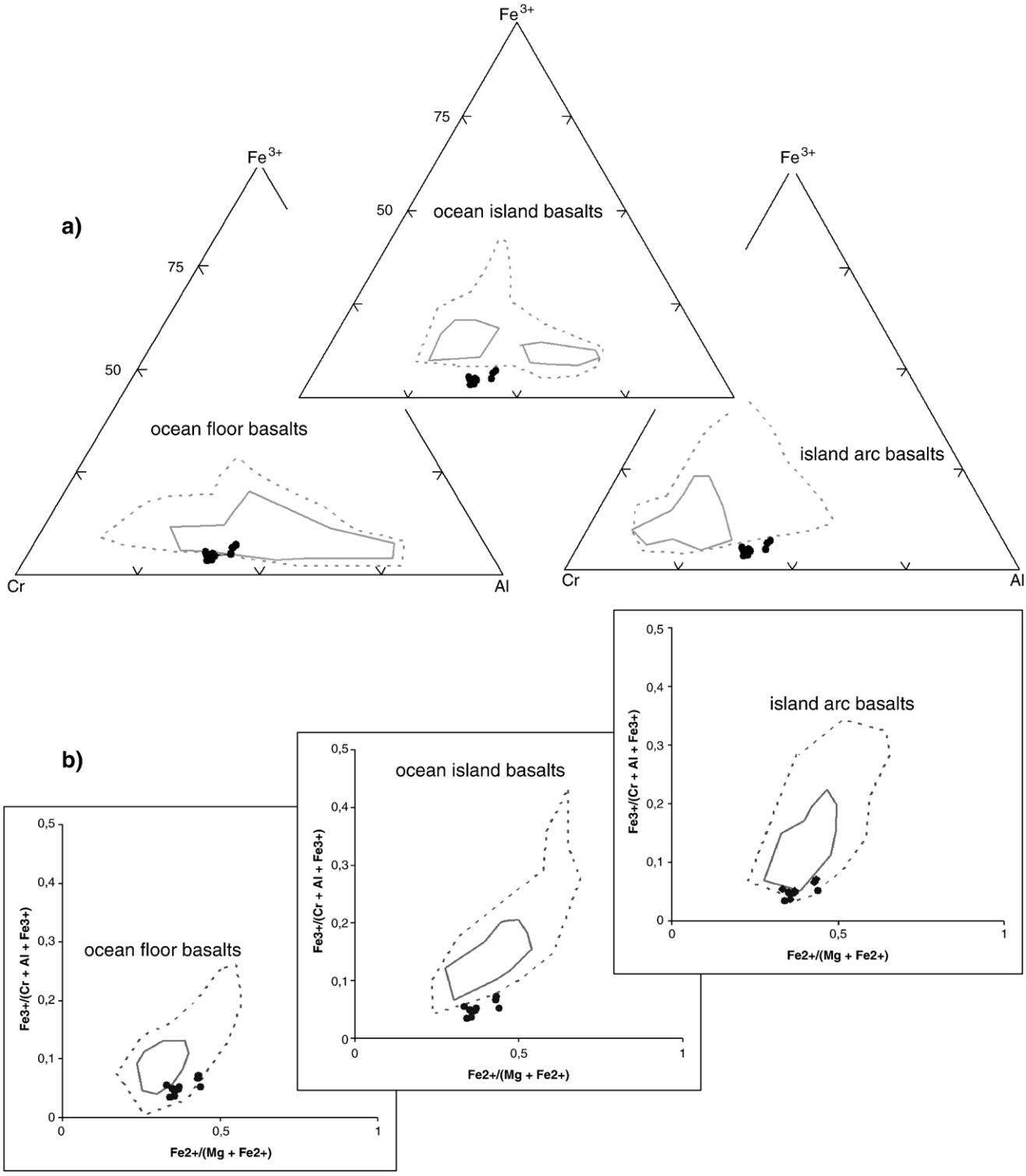

Fig. 5. Chromite plots. a) Trivalent ions plot for tholeiitic basalts, b) $Fe^{2+}/(Mg+Fe^{2+})$ vs. $Fe^{3+}/(Al+Cr+Fe^{3+})$. Heavy and dashed lines enclose the most densely packed 50% and 90% of all the data points taken from Barnes and Roeder (2001).

Roeder (2001) (Fig. 5a, b), while the augites plot in the non-alkaline basalts in the Leterrier et al. (1982) diagrams (Fig. 6a). Moreover, the (Ti+Cr) vs. Ca diagram of the latter authors permit to distinguish that the augites are more akin to those belonging to non-orogenic tholeiites (MORB and other tholeiites from spreading zones) (Fig. 6b).

The average of the DC metabasalts classifies as MORB in the trace element diagrams of Pearce and Norry (1979) and Pearce (1982) (Fig. 7a, b, c), although there is one sample (05–18) that plots very close to the limit between MORB and intra-plate basalt. The same sample shares characteristics of the within-plate tholeiites and within-plate alkali basalts in the diagram of Meschede (1986) (Fig. 7d). Even though MgO values have little meaning in such metamorphosed rocks, this sample is highly enriched in this oxide, and also in Ni and Cr relative to the other samples, and most likely represents a picritic basalt. The diagram of Meschede (1986) also allows the discrimination between the distinct types of ocean floor basalts, and although there is a strong scatter of the data between the N-MORB and E-MORB fields, the average of the DC analyses plot in the E-MORB field (Fig. 7d). It should be noted that there is concordance in the characterization of the schistose metabasaltic hyaloclastites classified as ocean floor basalts using the chemistry of their chromites, which also plot in the E-MORB field of Meschede (1986).

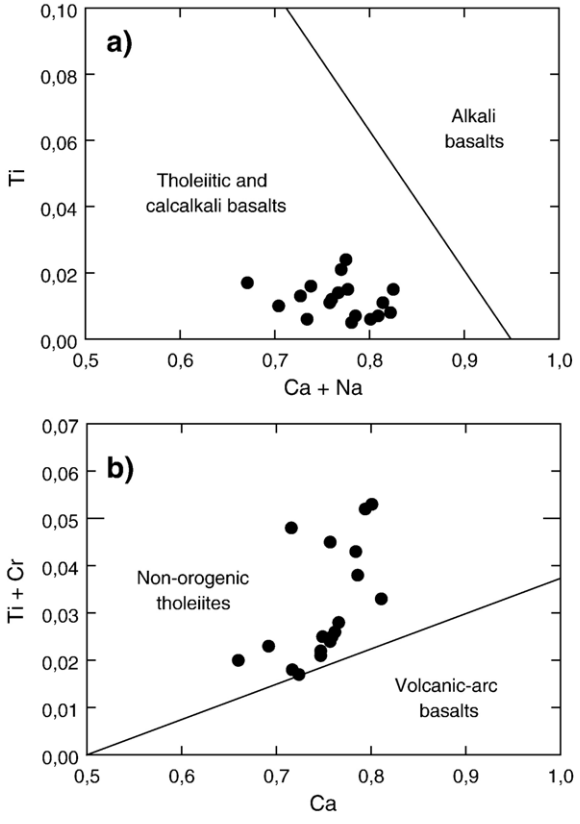

Fig. 6. Discrimination diagrams for clinopyroxenes (augites) phenocrystals in basalts (after Leterrier et al., 1982). Non-orogenic tholeiites includes MORB and other tholeiites from spreading zones (ocean-island tholeiites and back-arc basin tholeiites).

The whole rock analyses show that younger dykes cutting the whole MDT are tholeiitic andesites. On the diagrams of Pearce and Norry (1979) and Pearce (1982) they plot on the intra-plate field and the diagram of Meschede (1986) identify them as within-plate tholeiites or volcanic arc basalts (Fig. 7).

3.2. Metamorphic paragenesis and conditions

The general metamorphic mineral assemblage present in the DC metabasalts is albite–chlorite–epidote–pumpellyite–stilpnomelane–titanite (grothite)–garnet (grandite)–white mica–actinolite–titanomagnetite–quartz. Representative analyses of the metamorphic minerals of the metabasites from the DC are presented in Table 3. Pumpellyite exhibits considerable variations between those replacing the groundmass and those occurring in veinlets: crystals that replace the groundmass have greenish-brown pleocroism and X^{3+}_{Fe} [$Fe^{3+}/Fe^{3+}+Al_{total}$] of 10–19%, while those occurring in veinlets have bluish-green pleocroism and X^{3+}_{Fe} of 23–50%. Chlorite shows Si contents between 5.8 and 6.2 and *X*Fe [$Fe^{2+}/Fe^{2+}+Mg$] of 0.3–0.2. The absence of zeolites and prehnite suggests *P* and *T* conditions above 2 kbar and 260 °C (Frey et al., 1991), while the presence of stilpnomelane indicates *T* below 280 °C at ca. 2.5 kbar and below 330 °C at ca. 5 kbar (Massonne and Szpurka, 1997). The use of chlorite geothermometry (Cathelineau, 1988; Jowett, 1991) on the samples yields an average temperature of 259±11 °C, and the use of the Massonne and Szpurka (1997) geobarometer in white micas with high phengitic contents (Si=3.44–3.69 p.f.u.) indicates minimum pressures of 5 kb (Table 3).

4. Discussion and conclusions

Although the chromites have a more refractory and alteration resistant character than the clinopyroxenes (Barnes and Roeder, 2001) the tectonic discrimination diagrams based on the geochemistry of both relic igneous minerals give comparable results, indicating an environment of eruption of the DC basalts similar to the mid-ocean ridge basalts, in agreement with the whole rock geochemistry that indicates E-MORB characteristics. Interpretation of the whole rock chemical data is complicated by the metamorphic state of the samples, and for this reason only tectonic discrimination diagrams based on immobile trace elements were used, but it is probable that the scatter observed in these diagrams is produced by the fact that the concentrations of the more mobile elements were modified by open-system metamorphism. The results obtained for samples from different outcrops of the DC suggest that these basalts are similar to rocks formed as a bathymetrically elevated feature located at or near to a mid-oceanic spreading axis. An origin as an elevated ridge or plateau was also proposed for rocks with analogous characteristics in the Mino Terrane, Japan (Jones et al., 1993) and is additionally supported by the existence and extension of the coeval thick carbonate cover (TL).

The cross-cutting andesitic dykes have tholeiitic affinities and suggest an intra-continental plate origin. Structural field relationships and the unaltered and undeformed aspect indicate that these rocks were formed after the accretion and

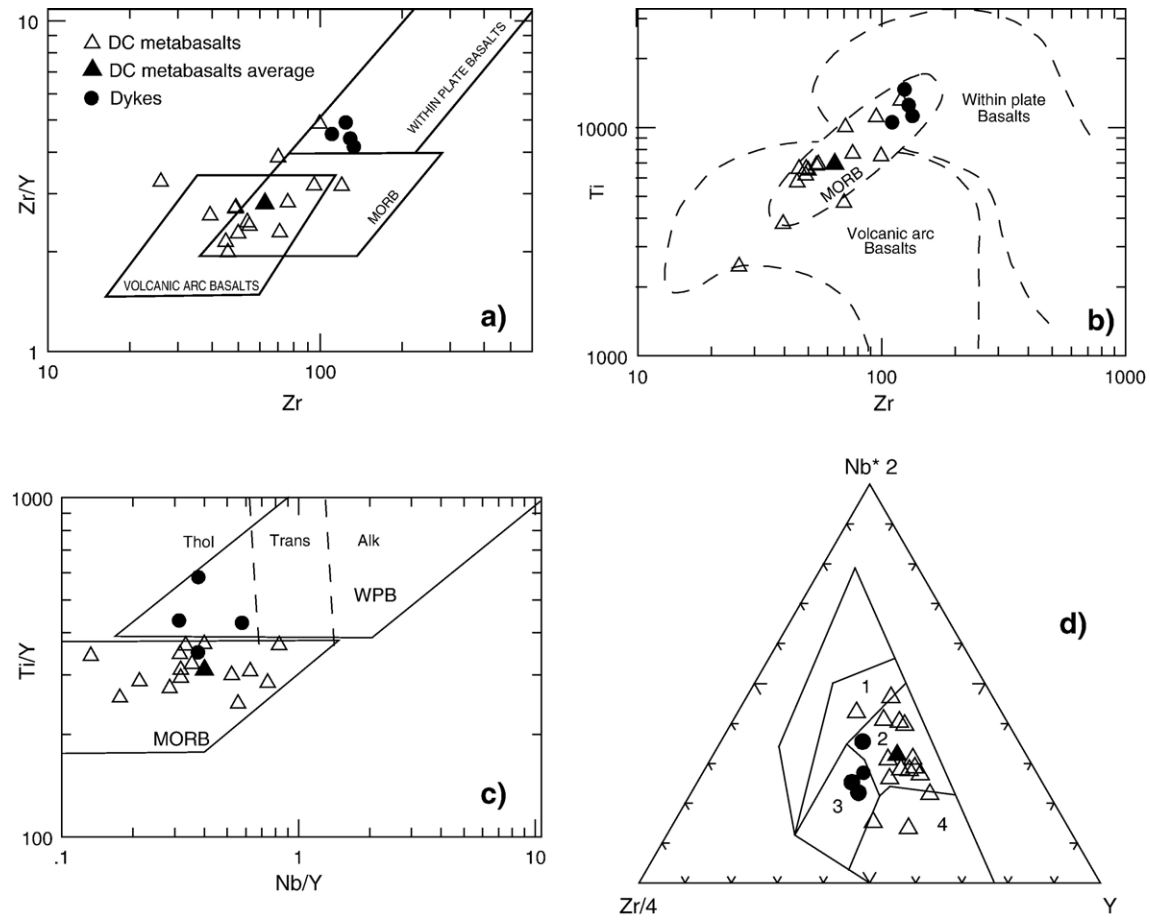

Fig. 7. Selected trace element discrimination diagrams. a) Zr vs. Zr/Y (Pearce and Norry, 1979); b) Zr vs. Ti (Pearce, 1982); c) Nb/Y vs. Ti/Y, showing the subdivision of the within plate basalts (Pearce, 1982); d) Ti–Zr–Y (Meschede, 1986). 1—within plate alkali basalts and within plate tholeiites, 2—E-type MORB, 3—within plate tholeiites and volcanic arc basalts, 4—N-type MORB and volcanic arc basalts.

metamorphism of the MDT. Duhart et al. (2003) described similar basaltic dykes in the Madre de Dios archipelago that cut both the SPB and the basement units. Apparently, this will suggest that the occurrence of basaltic dykes in the area is linked to the end phases of the intrusive igneous activity of the Patagonian Batholith, as previously indicated by Halpern (1973). Further work on geochemistry and geochronology is needed to reach a more reliable conclusion.

The presence of two different kinds of pumpellyites with markedly contrasting chemistry is best explained as indicative of equilibration of the system at (at least two) different *P–T* conditions. The stability field of the metamorphic mineral paragenesis and the thermo-barometric determinations indicate that the metamorphism of the DC took place under conditions of the pumpellyite–actinolite facies (Fig. 8), which has been observed to be present in accretionary prisms in Japan (Banno, 1998) and Chile (Hervé et al., 1999b; Willner et al., 2000). The development of this facies reveals that metamorphism took place under geothermal gradients between 10 and 20 °C/km, which might suggests slow subduction or subduction of young, relatively hot oceanic lithosphere (Hervé et al., 2007b). The conditions favourable for the development of this facies may have been generated during frontal accretion (off-scraping) of these rocks to the Gondwana margin, in a similar way as proposed by Willner et al. (2000) for the eastern belt of the Chonos Metamorphic Complex, which possibly formed during the same Late Triassic–Early Jurassic accretionary period as the DC. This period, known as Chonide event, has been attributed to a global reorganization of plates produced by the impact of mantle superplumes on the lithospheric plates (Vaughan and Livermore, 2005).

To prove the last hypothesis, it is necessary to have precise information on the time of docking of “suspect terranes” of similar lithology and depositional ages to the MDT, as the Le May Group in Alexander Island, Western Domain of the Antarctic Peninsula or the Torlesse Terrain in New Zealand (Lacassie et al., 2006; Hervé et al., 2006), clue areas along the Pacific margin of Gondwana. This will help to the evaluation of recently proposed hypotheses: that the accretionary events along the Gondwana margin are driven by oceanic subduction in a steady state mode, as suggested by Willner et al. (2004) for the Late Palaeozoic accretionary complex of south-central Chile, or that the accretionary events were episodic and related to the impact of superplumes (Vaughan and Livermore, 2005). Another aspect to be considered in future studies is that in spite of the indication by the metamorphic characteristics of the DC

Table 3
Representative microprobe analyses of selected metamorphic minerals

	White mica[1]							Chlorite[2]											Pumpellyite[3]					
	22	43	53	54	68	69		9803-6	9803-8	9803-42	9803-63	9803-80	9804-7	9804-14	9804-26	9804-76	9804-119		84_26	9803_3	9803_32	9803_85	9804_12	9804_84
SiO_2	53.71	53.47	55.06	53.82	53.75	54.11	SiO_2	29.44	29.66	29.98	27.90	29.16	30.18	29.71	31.10	30.47	28.88	SiO_2	37.75	35.88	35.17	36.32	34.91	37.20
TiO_2	0.04	0.02	0.02	0.01	0.03	0.02	Al_2O_3	17.80	17.07	17.62	16.05	18.44	15.82	16.66	17.35	17.02	15.67	TiO_2	0.10	0.09	0.01	0.03	0.12	0.04
Al_2O_3	13.05	13.56	22.35	22.20	12.74	24.55	FeO	17.30	16.98	16.71	16.78	16.43	12.71	12.45	12.03	12.16	12.35	Al_2O_3	24.47	22.05	13.79	22.98	14.02	23.76
Cr_2O_3	0.21	0.08	0.01	0.00	0.14	0.01	MnO	0.19	0.20	0.19	0.23	0.17	0.19	0.24	0.20	0.20	0.20	FeO*	4.13	8.38	20.15	7.02	19.24	4.60
FeO	11.86	11.11	5.77	6.75	11.66	4.45	MgO	22.10	22.31	22.50	20.42	22.53	25.38	24.84	25.74	26.07	24.79	Cr_2O_3	0.00	0.09	0.00	0.06	0.11	0.02
MnO	0.05	0.03	0.07	0.06	0.05	0.05	CaO	0.17	0.09	0.38	0.22	0.12	0.13	0.14	0.14	0.07	0.06	MnO	0.12	0.05	0.00	0.10	0.10	0.15
MgO	6.11	6.29	4.35	4.03	6.39	4.05	Na_2O	0.01	0.07	0.04	0.08	0.05	0.00	0.00	0.01	0.02	0.02	MgO	3.11	4.29	2.49	3.62	2.63	3.87
CaO	0.08	0.03	0.00	0.03	0.03	0.02	K_2O	0.03	0.02	0.08	0.03	0.03	0.02	0.01	0.01	0.03	0.02	CaO	22.15	21.59	22.12	22.67	21.99	23.46
Na_2O	0.02	0.02	0.01	0.01	0.00	0.02	TiO_2	0.02	0.02	0.01	0.03	0.02	0.02	0.03	0.07	0.02	0.01	Na_2O	0.03	0.04	0.02	0.03	0.02	0.04
K_2O	10.32	9.95	10.51	10.34	10.30	9.28	Cr_2O_3	0.06	0.07	0.06	4.46	0.00	2.97	2.05	0.29	0.15	3.89	K_2O	0.58	0.00	0.01	0.02	0.02	0.06
Total	95.44	94.56	98.16	97.26	95.11	96.55	Total	87.10	86.48	87.56	86.21	86.95	87.42	86.10	86.92	86.20	85.88	Total	92.44	92.44	93.75	92.83	93.14	93.20
Si	7.36	7.33	7.18	7.10	7.37	7.04	Si	5.87	6.04	5.88	5.93	5.81	6.01	5.99	6.13	6.00	6.05	Si	6.07	5.86	5.95	5.89	5.93	5.96
Al_{IV}	0.64	0.67	0.82	0.90	0.63	0.96	Al_{IV}	2.13	1.96	2.12	2.07	2.19	1.99	2.01	1.87	2.00	1.95	Ti	0.01	0.01	0.00	0.00	0.02	0.01
Sum_{IV}	8.00	8.00	8.00	8.00	8.00	8.00	Al_{VI}	2.05	2.14	1.95	1.96	2.13	1.72	1.95	2.16	1.96	1.92	Al	4.64	4.24	2.75	4.39	2.81	4.49
Al_{VI}	1.46	1.53	2.61	2.56	1.43	2.80	Fe^{2+}	2.88	2.89	2.74	2.98	2.74	2.12	2.10	1.98	2.00	2.16	Fe^{3+}	0.50	1.03	2.56	0.85	2.46	0.55
Ti	0.00	0.00	0.00	0.00	0.00	0.00	Mn	0.03	0.03	0.03	0.04	0.03	0.03	0.04	0.03	0.03	0.03	Cr^{3+}	0.00	0.01	0.00	0.01	0.01	0.00
Cr	0.02	0.01	0.00	0.00	0.02	0.00	Mg	6.57	6.78	6.57	6.47	6.69	7.53	7.46	7.56	7.66	7.74	Mn^{2+}	0.02	0.01	0.00	0.01	0.01	0.02
Fe^{2+}	0.42	0.35	0.63	0.61	0.37	0.48	Ca	0.04	0.02	0.08	0.05	0.03	0.03	0.03	0.03	0.01	0.01	Mg	0.75	1.04	0.63	0.88	0.67	0.93
Fe^{3+}	0.94	0.92	0.00	0.14	0.97	0.00	Na	0.00	0.03	0.02	0.03	0.02	0.00	0.00	0.00	0.01	0.01	Ca	3.81	3.78	4.01	3.94	4.00	4.03
Mn	0.01	0.00	0.01	0.01	0.01	0.01	K	0.01	0.00	0.02	0.01	0.01	0.00	0.00	0.00	0.01	0.00	Na	0.01	0.01	0.01	0.01	0.01	0.01
Mg	1.25	1.29	0.85	0.79	1.31	0.79	Ti	0.00	0.00	0.00	0.00	0.00	0.00	0.00	0.01	0.00	0.00	K	0.12	0.00	0.00	0.00	0.00	0.01
Sum_{VI}	4.10	4.10	4.10	4.10	4.10	4.08	Cr	0.01	0.01	0.01	0.75	0.00	0.47	0.33	0.04	0.02	0.64	Total	15.92	15.99	15.90	15.99	15.92	16.02
Ca	0.01	0.00	0.00	0.00	0.00	0.00	[4]T (°C)	266	253	256	291	278	259	263	239	249	280	XFe^{3+}	0.10	0.19	0.48	0.16	0.47	0.11
Na	0.00	0.01	0.00	0.00	0.00	0.00																		
K	1.80	1.74	1.75	1.74	1.80	1.54																		
Sum_{VIII}	1.82	1.75	1.75	1.75	1.81	1.55																		
OH	2.00	2.00	2.00	2.00	2.00	2.00																		

[1] The amounts of cations are based on 42 valencies neglecting the interlayer cations; the sum of octahedrally coordinated cations is set to 4.1 to allow for an estimation of Fe^{3+}.
[2] The amounts of cations are based on 28 oxygens; all Fe assumed to be Fe^{2+}.
[3] The amounts of cations are based on 24.5 oxygens. FeO* calculated by assuming FeO* = (Fe_2O_3 + 1.11*FeO); Fe^{3+} determined by using stoichiometry and an ideal $W_2XY_2Z_3O_{16.25}$ formula, where W=(Ca, Na, K, Mn); X=(Fe, Mg, Mn, Al, Cr); Y=(Ti, Fe, Al) and Z=(Si, Al).
[4] Temperature obtained using the Cathelineau's (1988) geothermometer.

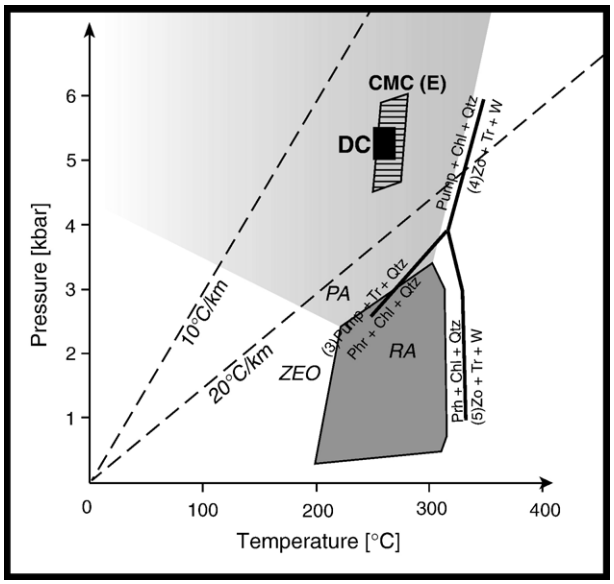

Fig. 8. Estimate of the *P–T* conditions of metamorphism. The black area is the supposed *P–T* conditions for the Denaro Complex (DC) (this work), and the dashed area is the *P–T* range for the eastern belt of Chonos Metamorphic Complex (CMC (E)) (taken from Willner et al. (2000)). The *P–T* field of ZEO (zeolite facies), PA (pumpellyite–actinolite facies), RA (prehnite–actinolite including prehnite–pumpellyite facies), and univariant reactions (3)–(5) (bold lines) are taken from Banno et al. (2000).

that it was emplaced in a subduction environment, there appears to be no coeval calc-alkaline magmatic arc in the Patagonian Andes or beyond.

Acknowledgements

A CONICYT doctoral grant to FS, support from Compañía de Aceros del Pacífico (CAP, Mina Guarello), Expedición Ultima Patagonia 2006 and Fondecyt projects 1010412 and 1050431 to FH have allowed field work and whole rock geochemistry. The first author specially thanks D. Quiroz, A. Vidal and S. Martini for fieldwork support. A German–Chilean BMBF-CONICYT cooperation project Chl 01A 6A "High pressure metamorphic rocks in Chile" has allowed microprobe analysis at Stuttgart Universität under the guidance of H. Massonne and T. Theye. The Paleomineralization Group at Johannesburg University has provided the XRF geochemistry. A. Vaughan and A. Willner are also thanked for their useful comments. Reviews by Drs. H.-J. Massonne, J. Bradshaw and R.A.J. Trouw greatly improved the manuscript.

References

Arai, S., 1992. Chemistry of chromian spinel in volcanic rocks as a potential guide to magma chemistry. Mineralogical Magazine 56, 173–184.

Banno, S., 1998. Pumpellyite–actinolite facies of the Sanbawaga metamorphism. Journal of Metamorphic Geology 16, 117–128.

Banno, S., Toriumi, M., Obata, M., Nishiyama, T., 2000. Dynamics of Petrogenesis. University of Tokyo Press, Tokyo.

Barnes, S.J., Roeder, P.L., 2001. The range of spinel composition in terrestrial mafic and ultramafic rocks. Journal of Petrology 42, 2279–2302.

Bruce, R., Nelson, E., Weaver, S., Lux, D., 1991. Temporal and spatial variations in the Southern Patagonian Batholith; constrains on magmatic arc development. Geological Society of America, Special Paper 265, 1–12.

Cathelineau, M., 1988. Cation site occupancy in chlorites and illites as a function of temperature. Clay Minerals 23, 471–485.

Cawood, P.A., Landis, C.A., Nemchin, A.A., Hada, S., 2002. Permian fragmentation, accretion and subsequent translation of a low-latitude Tethyan seamount to the high-latitude east Gondwana margin: evidence from detrital zircon age data. Geological Magazine 139, 131–144.

Ceccioni, G., 1956. Primeras noticias sobre la existencia del Paleozoico Superior en el Archipiélago Patagónico entre los paralelos 50° y 52° S. Universidad de Chile, Facultad de Ciencias Físicas y Matemáticas, Anales 13, 183–202.

Douglass, R.C., Nestell, M.K., 1976. Late Paleozoic Foraminifera from southern Chile. U.S. Geological Survey Professional Paper 858, 1–47.

Duhart, P., Muñoz, J., Tassinari, C., Quiroz, D., 2003. K–Ar Geochronology and Sr and Nd isotopic composition of the Patagonian Batholith in the Madre de Dios Archipelago (50° 30′ S), Southern Chile. IV South American Symposium on Isotope Geology. Salvador, Bahía, Brasil.

Forsythe, R.D., 1982. The late Palaeozoic to early Mesozoic evolution of southern South America: a plate tectonic interpretation. Journal of the Geological Society of London 139, 671–682.

Forsythe, R.D., Mpodozis, C., 1979. El Archipiélago Madre de Dios, Patagonia occidental, Magallanes. Aspectos generales de la estratigrafía y estructura del basamento pre-Jurásico Superior. Instituto de Investigaciones Geológicas, Revista Geológica de Chile 7, 13–29.

Forsythe, R.D., Mpodozis, C., 1983. Geología del Basamento pre-Jurásico Superior en el Archipiélago Madre de Dios, Magallanes, Chile. Servicio Nacional de Geología y Minería, Boletín, vol. 39. 63 pp.

Frey, M., De Capitani, C., Liou, J.G., 1991. A new petrogenetic grid for low-grade metabasites. Journal of Metamorphic Geology 9, 497–509.

Hada, S., Ishii, K., Landis, C.A., Aitchinson, J., Yoshikura, S., 2001. Kurosegawa Terrane in Southwest Japan: disrupted remnants of a Gondwana-derived terrane. Gondwana Research 4, 27–38.

Halpern, M., 1973. Regional Geochronology of Chile south of 50° latitude. Geological Society of America Bulletin 84, 2407–2422.

Hervé, F., Mpodozis, C., 2005. The western Patagonia terrane collage: new facts and some thought-provoking possibilities. In: Pankhurst, R.J., Veiga, G.D. (Eds.), Gondwana-12, Geological and Biological heritage of Gondwana, Abstracts, Mendoza, Argentina.

Hervé, F., Fanning, M., Bradshaw, J., Bradshaw, M., Lacassie, J.P., 1999a. Late Permian SHRIMP U–Pb detrital zircon ages constrain the age of accretion of oceanic basalts to the Gondwana margin at the Madre de Dios Archipelago, southern Chile. 4th International Symposium on Andean Geodynamics, Extended Abstracts Volume. IRD, Göttingen, Paris, pp. 327–328.

Hervé, F., Aguirre, L., Sepúlveda, V., Morata, D., 1999b. Contrasting geochemistry and metamorphism of pillow basalts in metamorphic complexes from Aysen, S. Chile. Journal of South American Earth Sciences 12, 379–388.

Hervé, F., Pankhurst, R.J., Spiro, B., Yi, Liu Dun, 2000. Limestones of southern Chile: preliminary isotopic investigation and implications. IX Congreso Geológico Chileno, Actas, vol. II. Sociedad Geológica de Chile, Puerto Varas, Santiago, pp. 736–737.

Hervé, F., Miller, H., Pimpirev, C., 2006. Patagonia–Antarctica connections before Gondwana break-up. In: Fütterer, D.K., Damaske, D., Kleinschmidt, G., Miller, H., Tessensohn, F. (Eds.), Antarctica: Contributions to Global Earth Sciences. Springer–Verlag, Berlin Heidelberg, pp. 217–228.

Hervé, F., Pankhurst, R.J., Fanning, C.M., 2003. Detrital zircon ages patterns and provenance of the metamorphic complexes of southern Chile. Journal of South American Earth Sciences 16, 107–123.

Hervé, F., Pankhurst, R.J., Fanning, C.M., Calderón, M., Yaxley, G.M., 2007a. The South Patagonian batholith: 150 my of granite magmatism on a plate margin. Lithos, doi:10.1016/j.lithos.2007.01.007, 22 pages.

Hervé, F., Faúndez, V., Calderón, M., Massonne, H.J., Willner, A.P., 2007b. Metamorphic and plutonic basement complexes. In: Moreno, T., Gibbons, W. (Eds.), The Geology of Chile. Geological Society, London, Special Publications, pp. 5–19.

Jones, G., Sano, H., Valsami-Jones, E., 1993. Nature and tectonic setting of accreted basalts from the Mino terrane, central Japan. Journal of the Geological Society of London 150, 1167–1181.

Jowett, E.C., 1991. Fitting iron and magnesium into the hydrothermal chlorite geothermometer. GAC/MAC/SEG Joint Annual Meeting (Toronto, May 27–29, 1991), Program with Abstracts, vol. 16, p. A62.

Lacassie, J.P., 2003. Estudio de la proveniencia sedimentaria de los complejos metamórficos de los Andes Patagónicos (46°–51° Lat. S) mediante la aplicación de redes neuronales e isótopos estables. PhD thesis, Departamento de Geología, Universidad de Chile.

Lacassie, J.P., Roser, B., Hervé, F., 2006. Sedimentary provenance study of the post-Early Permian to pre-Early Cretaceous Duque de York Complex, Chile. Revista Geológica de Chile 33, 199–219.

Leterrier, J., Maury, R.C., Thonon, P., Girard, D., Marchal, M., 1982. Clinopyroxene composition as a method of identification of the magmatic affinities of paleo-volcanic series. Earth and Planetary Science Letters 59, 139–154.

Ling, H.Y., Forsythe, R.D., Douglass, C.R., 1985. Late Paleozoic microfaunas from Southernmost Chile and their relation to Gondwanaland forearc development. Geology 13, 357–360.

Massonne, H.J., Szpurka, Z., 1997. Thermodynamic properties of white mica on the basis of high-pressure experiments in the systems K_2O–MgO–Al_2O_3–Si_2O–H_2O and K_2O–FeO–Al_2O_3–Si_2O–H_2O. Lithos 41, 229–250.

Meschede, M., 1986. A method of discriminating between different types of mid-ocean ridge basalts and continental tholeiites with the Nb–Zr–Y diagram. Chemical Geology 56, 207–218.

Pankhurst, R.J., Weaver, S.D., Hervé, F., Larrondo, P., 1999. Mesozoic–Cenozoic evolution of the North Patagonian Batholith in Aysén, southern Chile. Journal of the Geological Society of London 156, 673–694.

Pearce, J.A., 1982. Trace elements characteristics of lavas from destructive plate boundaries. In: Thorpe, R.S. (Ed.), Andesites. Wiley, Chichester, pp. 525–548.

Pearce, J.A., Norry, M.J., 1979. Petrogenetic implications of Ti, Zr Y and Nb variations in volcanic rocks. Contributions to Mineralogy and Petrology 69, 33–47.

Rapalini, A.E., Hervé, F., Ramos, V.A., Singer, S.E., 2001. Paleomagnetic evidence for a very large counterclockwise rotation of the Madre de Dios Archipelago, southern Chile. Earth and Planetary Science Letters 184, 471–487.

Sepúlveda, F., 2004. Metamorfismo de bajo grado en rocas del Complejo Denaro, archipiélago Madre de Dios, XII región. Graduation thesis, Departamento de Geología, Universidad de Chile.

Thomson, S.N., Hervé, F., 2002. New time constraints for the age of metamorphism at the ancestral Pacific Gondwana margin of southern Chile (42–52° S). Revista Geológica de Chile 29, 255–271.

Vaughan, A.P.M., Livermore, R.A., 2005. Episodicity of Mesozoic terrane accretion along the Pacific margin of Gondwana: implications for superplume–plate interactions. In: Vaughan, A.P.M., Leat, P.T., Pankhurst, R.J. (Eds.), Terrane Processes at the Margins of Gondwana. Geological Society, London, Special Publications, vol. 246, pp. 143–178.

Willner, A., Hervé, F., Massonne, H.J., 2000. Mineral chemistry and pressure–temperature evolution of two contrasting high-pressure–low-temperature belts in the Chonos Archipelago, Southern Chile. Journal of Petrology 41, 309–330.

Willner, A.P., Glodny, J., Gerya, T.V., Godoy, E., Massonne, H.-J., 2004. A counterclockwise PTt path of high-pressure/low-temperature rocks from the Coastal Cordillera accretionary complex of south-central Chile: constraints for the earliest stage of subduction mass flow. Lithos 75, 283–310.